A TRIDENT SCHOLAR PROJECT REPORT

NO. 448

Dead-Zone Oscillator Control for Communication-Free Synchronization of Paralleled, Three-Phase, Current-Controlled Inverters

by

Midshipman 1/C Spencer C. Shabshab, USN

UNITED STATES NAVAL ACADEMY
ANNAPOLIS, MARYLAND

USNA-1531-2

U.S.N.A. --- Trident Scholar project report; no. 448 (2016)

Dead-Zone Oscillator Control for Communication-Free Synchronization Of Paralleled, Three-Phase, Current-Controlled Inverters

by

Midshipman 1/C Spencer C. Shabshab
United States Naval Academy
Annapolis, Maryland

_____
(signature)

Certification of Adviser(s) Approval

Assistant Professor Daniel F. Opila
Electrical and Computer Engineering Department

_____
(signature)

_____
(date)

CDR John D. Stevens, USN
Electrical and Computer Engineering Department

_____
(signature)

_____
(date)

Acceptance for the Trident Scholar Committee

Professor Maria J. Schroeder
Associate Director of Midshipman Research

_____
(signature)

_____
(date)

USNA-1531-2

REPORT DOCUMENTATION PAGE

Form Approved
OMB No. 0704-0188

1. REPORT DATE *(DD-MM-YYYY)*	**2. REPORT TYPE**	**3. DATES COVERED** *(From - To)*
05-11-2016		

4. TITLE AND SUBTITLE

Dead-Zone Oscillator Control for Communication-Free Synchronization of Paralleled, Three-Phase, Current-Controlled Inverters

5a. CONTRACT NUMBER

5b. GRANT NUMBER

5c. PROGRAM ELEMENT NUMBER

6. AUTHOR(S)
Shabshab, Spencer C.

5d. PROJECT NUMBER

5e. TASK NUMBER

5f. WORK UNIT NUMBER

7. PERFORMING ORGANIZATION NAME(S) AND ADDRESS(ES)

8. PERFORMING ORGANIZATION REPORT NUMBER

9. SPONSORING / MONITORING AGENCY NAME(S) AND ADDRESS(ES)
U.S. Naval Academy
Annapolis, MD 21402

10. SPONSOR/MONITOR'S ACRONYM(S)

11. SPONSOR/MONITOR'S REPORT NUMBER(S)
Trident Scholar Report no. 448 (2016)

12. DISTRIBUTION / AVAILABILITY STATEMENT

This document has been approved for public release; its distribution is UNLIMITED.

13. SUPPLEMENTARY NOTES

14. ABSTRACT

The prevalence of converter-interfaced power sources in the power grids of both civilian and military systems is increasing due to technological improvements in power conversion and changing requirements in system loads. The development of high-power pulsed loads on naval platforms, such as the Laser Weapon System (LaWS) and the electromagnetic railgun, calls for the ability to rapidly and drastically change the allocation of power in a system that contains many other loads.

A new method of synchronizing parallel-connected converter-interfaced power sources, which involves controlling converters to emulate the dynamics of a nonlinear dead-zone oscillator, may provide an advantage. This method, termed Virtual Oscillator Control (VOC), was previously tested and validated for networks of single-phase, voltage-source power converters and supported in simulation for networks of three-phase, voltage-source inverters. The effectiveness of VOC in the control of three-phase grids was here validated through hardware experimentation. Additionally, VOC was extended to implementation with current-controlled inverters, which are very prevalent in power systems because of their enhanced safety and circuit-protection features. The hardware validation and performance evaluation of VOC applied to networks of parallel-connected, three-phase, current-controlled inverters is here detailed.

15. SUBJECT TERMS
power converters, virtual oscillators, inverter synchronization, converter control, inverter control, microgrid

16. SECURITY CLASSIFICATION OF:			**17. LIMITATION OF ABSTRACT**	**18. NUMBER OF PAGES**	**19a. NAME OF RESPONSIBLE PERSON**
a. REPORT	**b. ABSTRACT**	**c. THIS PAGE**		23	**19b. TELEPHONE NUMBER** *(include area code)*

Abstract

The prevalence of converter-interfaced power sources in the power grids of both civilian and military systems is increasing due to technological improvements in power conversion and changing requirements in system loads. In the civilian sector this increase in prevalence is driven in part by the increasing attractiveness of renewable and small-scale alternatives to the terrestrial power grid that has traditionally powered homes, offices, and facilities. In the military, power conversion is being integrated primarily because it is receptive to automatic control and allows more manipulation of power distribution. The development of high-power pulsed loads on naval platforms, such as the Laser Weapon System (LaWS) and the electromagnetic railgun, calls for the ability to rapidly and drastically change the allocation of power in a system that contains many other loads. The increased penetration of converter-interfaced sources has led to the emergence of a new control problem: the synchronization of parallel-connected, converter-interfaced AC sources. The electromechanical drives that have traditionally dominated power systems have physical properties and operating dynamics that naturally aid synchronization. In power systems that feature a high penetration of converter-interfaced sources, the dynamics of which are determined directly by control rather than by their physical properties, the task of synchronization must be accomplished through control. Existing solutions to this control problem typically require an overlying communication network between converters to perform optimally. Because a centralized communication network introduces a single point of failure into the power system, it would be advantageous if synchronization could be satisfactorily achieved without it. A new method of synchronizing parallel-connected converter-interfaced power sources, which involves controlling converters to emulate the dynamics of a nonlinear dead-zone oscillator, may provide this advantage. This method, termed Virtual Oscillator Control (VOC), was previously tested and validated for networks of single-phase, voltage-source power converters and supported in simulation for networks of three-phase, voltage-source inverters. The effectiveness of VOC in the control of three-phase grids was here validated through hardware experimentation. Additionally, VOC was extended to implementation with current-controlled inverters, which are very prevalent in power systems because of their enhanced safety and circuit-protection features. The hardware validation and performance evaluation of VOC applied to networks of parallel-connected, three-phase, current-controlled inverters is here detailed.

Keywords: power converters, virtual oscillators, inverter synchronization, converter control, inverter control, microgrid

Acknowledgments

I would first like to acknowledge my project advisors, Asst. Professor Daniel F. Opila and CDR John Stevens of the Naval Academy's Electrical and Computer Engineering Department, for their diligent and patient mentorship.

Asst. Professor Daniel F. Opila was a driving force behind the extension of voltage-source algorithms to current-controlled devices, and contributed significantly to the theoretical development of that method.

Dr. Brian B. Johnson, Dr. Sairaj V. Dhople, Dr. James L. Cale, Dr. Abdullah O. Hamadeh, and Dr. Phillip T. Krein, for providing the inspiration, theoretical basis, and conceptual footholds necessary to take up this project, are owed inestimable acknowledgment and thanks.

This work was greatly facilitated by the always-enthusiastic support of the Naval Academy Electrical and Computer Engineering Department technical support team.

Contents

1 Introduction

The ever-increasing energy demands of individuals, industry, and nations have historically been satisfied in large part by the expansion and improvement of geographically enormous terrestrial power grids. Such grids primarily utilize electromechanical power sources, such as large natural gas or steam turbines. The interaction between such power sources when they are electrically coupled to provide power simultaneously to a common load is determined by the physical and electrical properties of the machines themselves, and also by those of the grid to which they are connected. Methods of integrating and controlling such power sources to provide power to a common load are well-formulated. Recently, however, pockets of society, industry, and national infrastructure have begun to move toward the use of smaller grids that generate and distribute power from renewable resources over a relatively small geographical area. Along with an increased prevalence of renewable resources comes greater penetration of power-conversion technology to convert the power produced by renewables into a form acceptable for consumption. The desired behaviors of converter-interfaced systems are the same as those of the legacy power grid, but achieving them is more difficult.

In general, we desire parallel power sources to provide power in proportion to their ratings, such that a low-capacity source provides less power than a high capacity source. In alternating-current (AC) systems, another important performance requirement is that parallel power sources be synchronized so that they work in concert to provide power to their common load [1]. Synchronization is illustrated both negatively and positively in Figure 1. Load-sharing and synchronization are relatively easy to achieve in systems of coupled electromechanical generators because the dynamics of those machines are naturally conducive to the desired behaviors. It is less straightforward to achieve the same behavior in systems of parallel, converter-interfaced sources because the dynamics of converters are determined almost entirely by control rather than by their electrical and physical properties. The dynamic manipulability of power converter dynamics therefore presents both opportunity and challenge, the freedom to define source dynamics being balanced by the loss of natural electromechanical properties that previously facilitated load-sharing and synchronization [2, 3, 4]. Control methods that ensure synchronization and load-sharing in AC power systems of parallel-connected inverters (converters that produce an AC output) have traditionally involved controlling the inverters to emulate electromechanical generator dynamics. One example of this is called droop control [5].

An emerging family of control methods involves controlling inverters to emulate the dynamics of various virtual oscillators, the dynamics of which differ from those of electromechanical generators and potentially offer performance benefits [6, 7]. This general method is called "Virtual Oscillator Control" (VOC). One member of the VOC family is Dead-Zone Oscillator (DZO) control, which entails controlling inverters to emulate the dynamics of the nonlinear DZO.

DZO control was formulated for voltage-source inverters (inverters that modulate their switching patterns such that their output voltages follow a reference signal), and previously has only been implemented with voltage-source inverters. However, current-controlled converters are more common today because they facilitate output-limiting for safety and circuit protection. DZO control has previously only been experimentally validated for single-phase inverters (inverters that have one power output), but many power systems today utilize three-phase power sources (sources which have three power outputs which are phase separated by 120^o). This paper attempts to facilitate the deployment of DZO control by extending it to current-controlled inverters, demonstrating a load-

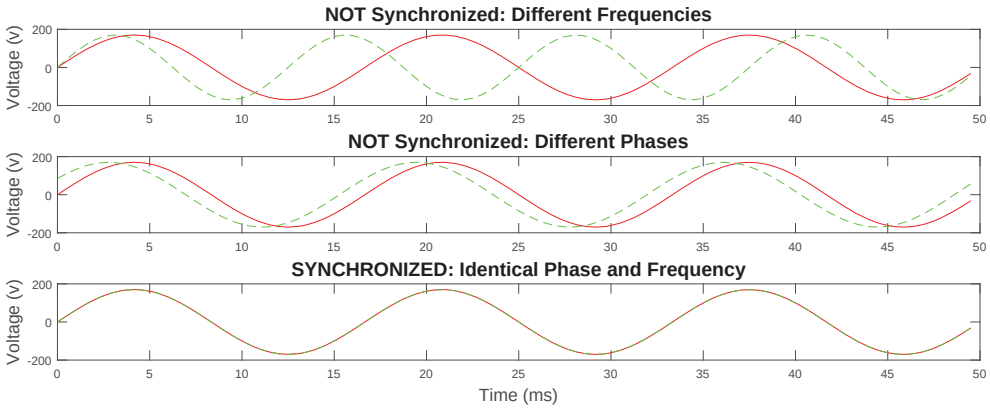

Figure 1: From top to bottom: Two illustrations of waveforms that are not synchronized and one of waveforms that are synchronized.

sharing adjustment method unique to DZO control of current-controlled inverters, and validating its effectiveness in three-phase systems through hardware testing for the first time.

2 Previous Work

Dead-Zone Oscillator (DZO) control is a member of the virtual oscillator control family that entails controlling inverters to emulate the dynamics of a nonlinear DZO. The primary performance benefits of DZO control are the communicationless synchronization of parallel-connected inverters and multiple practical methods by which to control load-sharing. In [8], DZO control was presented as a novel way to synchronize single-phase systems of parallel-connected voltage-source inverters, and a method was developed to control load-sharing between inverters by altering the impedances of their physical output filters. In [5], DZO control was experimentally validated in a single-phase system and sufficient conditions for the self-synchronization of parallel inverters were derived. The extension of DZO control to a three-phase system of parallel-connected voltage-source inverters was introduced and simulated in [9], and a method of controlling the relative power contribution of inverters by altering their current feedback gains was introduced.

2.1 The Dead-Zone Oscillator

The nonlinear dead-zone oscillator (DZO) is a mathematical construct used to describe the behavior of several real-world systems that are observed in fields ranging from biology, physics, and chemistry to social networks [10]. The electrical circuit-equivalent of the Dead-Zone oscillator is shown in Figure 2 [8].

The voltage-dependent current source $g(V_{osc})$ in Figure 2 is the source of the DZO's nonlinear dynamics, and has characteristics described by Figure 3 and (1) [8]:

$$g(V_{osc}) = f(V_{osc}) - \sigma V_{osc} \tag{1}$$

Where σ is a parameter of $f(V_{osc})$, the dead-zone function and namesake of DZO control, which is described by Figure 4 and (2) [8]:

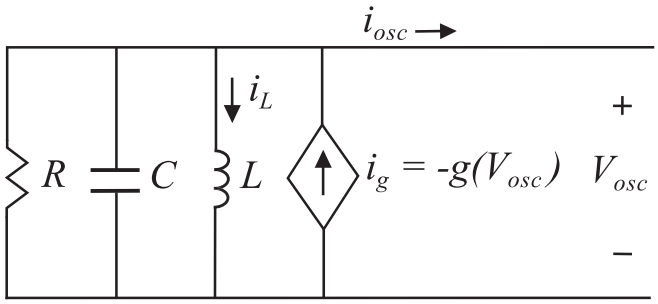

Figure 2: An electrical model of the nonlinear dead-zone oscillator. The symbols labeled R, L, and C, represent an electrical resistor, inductor, and capacitor, respectively. Terms that include I represent electrical currents, and V terms represent electrical voltages.

$$f(V_{osc}) = \begin{cases} 2\sigma(V_{osc} - \varphi), & V_{osc} > \varphi \\ 0, & |V_{osc}| \leq \varphi \\ 2\sigma(V_{osc} + \varphi), & V_{osc} < -\varphi \end{cases} \tag{2}$$

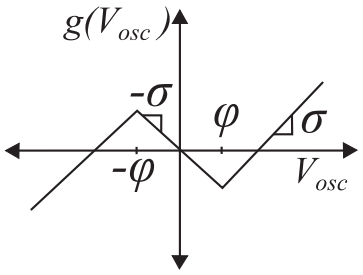

Figure 3: The voltage-current characteristic of the DZO circuit's voltage-dependent current source.

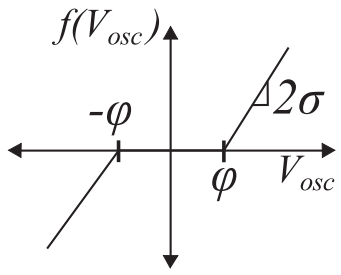

Figure 4: The dead-zone function. Parameters φ and σ determine the breadth of the "dead-zone" and the slope of $f(V_{osc})$, respectively.

The dead-zone oscillator is thus a nonlinear dynamic system of two states: The inductor current i_L and the DZO terminal voltage V_{osc}. The dynamics of the dead-zone oscillator are summarized by (3) and (4) [8]:

$$\frac{dV_{osc}}{dt} = \frac{1}{C}\left[V_{osc}(\sigma - \frac{1}{R}) - f(V_{osc}) - i_L - i_{osc}\right] \tag{3}$$

$$\frac{di_L}{dt} = \frac{1}{L}V_{osc}, \tag{4}$$

The dynamics of the DZO as described in (3) and (4) are straightforward to compute as a first-order state model of V_{osc} and i_L, with input i_{osc} and output V_{osc}. In [8]-[9], V_{osc} is scaled to create a control signal that causes a voltage-source inverter to emulate DZO dynamics. (3) can be algebraically changed to (5), such that the input to the DZO state model is V_{osc} and its output is i_{osc}:

$$i_{osc} = -g(V_{osc}) - i_L - \frac{V_{osc}}{R} - C\frac{dV_{osc}}{dt} \tag{5}$$

When (5) is evaluated instead of (3), the state model output i_{osc} can be used as the reference signal for a current-controlled inverter. However, (5) is difficult to accurately evaluate for real systems because channel noise makes differentiating V_{osc} prone to significant error. Thus, it is not straightforward to generate a control signal for a current-controlled inverter directly from the DZO model of Figure 2.

2.2 DZO characteristics

The dynamics of the DZO, both in isolation and when coupled to other oscillators, is determined by the values of R, L, C, φ, and σ. Significant work was dedicated in [8]-[9] to determining how the selection of these parameters affects DZO dynamics. It was shown in [8] that V_{osc} for a DZO with nothing connected to its terminals, such that $i_{osc} = 0$, converges on a unique and stable limit cycle if $\sigma > \frac{1}{R}$. Convergence of V_{osc} to a unique and stable limit cycle means that the voltage will reach a steady-state AC oscillation, though not necessary a sinusoidal oscillation, at a frequency approximately equal to the natural frequency of the DZO's parallel RLC circuit: $1/\sqrt{LC}$. It was also shown in [8] that the limit cycle of V_{osc} approached sinusoidal oscillation when $\sqrt{L/C}(\sigma - 1/R) \ll 1$. Thus, the parameters of a DZO can be selected such that it functions as a sinusoidal AC voltage source.

2.3 DZO control of voltage-source inverters

DZO control of a voltage-source inverter entails scaling the oscillator voltage V_{osc} by ν to produce the commanded inverter terminal voltage V_i [8]. The simulated DZO is driven by the real current measured at the inverter output, I_F, scaled by ι.

$$V_i = \nu v_{osc}, \tag{6}$$

$$i_{osc} = \iota I_F. \tag{7}$$

The controller simulates (3) and (4), converting the measured I_F to the DZO state model input i_{osc} and extracting the terminal voltage v_{osc} as outlined in (6) and (7). This control process is illustrated in Figure 5. When inverters are parallel-connected under DZO control the output current of the k^{th} inverter is determined by $V_{i,k}$, $F_{s,k}$, and V_G, the voltage on the system's load. The inverters self-synchronize due to the dependence of each current $I_{F,k}$ on the shared grid voltage. Load-sharing between inverters is accomplished through the dependence of each inverter current $I_{F,k}$ on its own output filter impedance $F_{s,k}$.

A sufficient condition for the synchronization of any number of parallel-connected inverters under DZO control was derived in [5]:

$$\sup_{\omega\in\mathbb{R}} \left|\left| \frac{(\iota\nu)^{-1} Z_{F,R}(j\omega) Z_{osc}(j\omega)}{(\iota\nu)^{-1} Z_{F,R}(j\omega) + Z_{osc}(j\omega)} \right|\right|_2 \sigma < 1 \tag{8}$$

Where Z_{osc} is the impedance of the DZO's resonant RLC circuit and $Z_{F,R}$ is a linear reference filter impedance to which any k^{th} inverter's output impedance is constrained to be proportional by a factor of κ_k^{-1}. In this case, computing $F_{s,k}$ involves calculating the current through the output

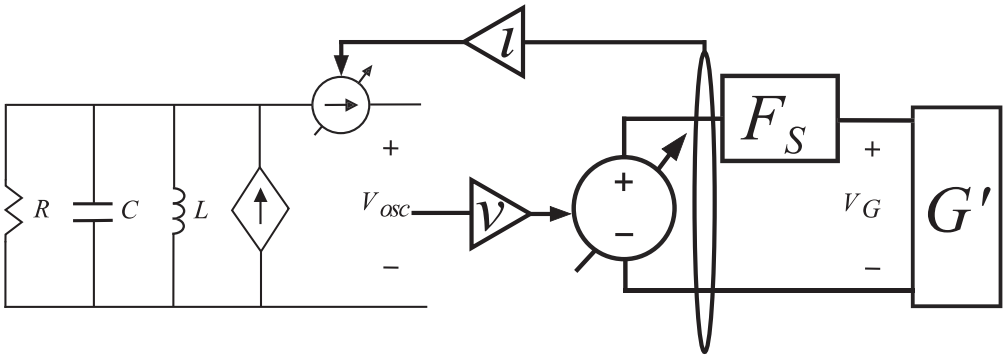

Figure 5: To exercise DZO control of a voltage-source inverter, the measured inverter output current is scaled by ι to produce the virtual DZO current i_{osc} and V_{osc} is scaled by ν to produce the inverter reference voltage.

impedance of the k^{th} inverter, which is given by $\kappa_k^{-1} Z_{F,R}$.

It is also demonstrated in [8] that the relative power contributions of synchronized inverters under DZO control are related to the relative output impedances of the inverters as stated in (9):

$$\frac{P_k}{P_j} = \frac{\kappa_j}{\kappa_k} \qquad \forall k, j = 1...N \tag{9}$$

Parallel voltage-source inverters controlled as illustrated in Figure 5 with DZO parameters that satisfy (8) are guaranteed to synchronize if both DZO simulation and voltage-source control are much faster than the fastest system dynamic. Under DZO control and subject to these conditions, the relative power contributions of inverters can be altered by changing their output impedances according to (9) [8]. Attaining the result of (9) for parallel voltage-source inverters requires physically changing the filter impedance at the output of an inverter. The relative power contribution of an inverter under DZO control can also be altered by changing ι, as developed in [9].

2.4 Extension of DZO control to three-phase systems

In [9], a method of applying DZO control to three-phase voltage-source inverters was presented. This method involves simulating DZO dynamics on just one phase of each inverter, and using the inverse-$\alpha\beta$ coordinate transform to generate a three-phase control signal based on V_{osc} and i_L of the DZO. The inverse-$\alpha\beta$ coordinate transform can be summarized as the matrix multiplication of two signals, f_α and f_β, to generate signals f_A, f_B, and f_C. If f_α and f_β are orthogonal signals and $|f_\alpha| = |f_\beta|$, then f_A, f_B, and f_C form a balanced three-phase set of signals as in (10) [11].

$$\begin{bmatrix} 1 & 0 \\ -\frac{1}{2} & \frac{\sqrt{3}}{2} \\ -\frac{1}{2} & -\frac{\sqrt{3}}{2} \end{bmatrix} \begin{bmatrix} V_{osc} \\ \sqrt{\frac{L}{C}} i_L \end{bmatrix} \nu = \begin{bmatrix} V_{i,A} = \nu V_{osc} \\ V_{i,B} = V_{i,A} \angle -120^\circ \\ V_{i,C} = V_{i,A} \angle -240^\circ \end{bmatrix} \tag{10}$$

If the DZO parameters are selected such that it oscillates in an approximately sinusoidal limit cycle as described in Section 2.2, then a set of balanced three-phase reference voltages can be generated from V_{osc} and i_L of each inverter's simulated DZO by applying the inverse-$\alpha\beta$ transform. Note that V_{osc} is "fed-through" the $\alpha\beta$ transformation such that $V_{i,A}$, the voltage reference for the inverter's A-phase, is controlled to emulate the simulated DZO dynamics in the same manner as was described for single-phase inverters in (6) and (7). Three-phase DZO control exercised in this way is identical to the single-phase case, except that there are two additional outputs, $V_{i,B}$ and $V_{i,C}$, which depend on the same simulated oscillator.

3 Current-Controlled Equivalent of A Voltage-Source Algorithm

DZO control was developed in [8]-[9] for application to voltage-source inverters, but current-controlled inverters are more prevalent in power systems because they are capable of implementing protective output current limits in the case of short circuits. DZO control would be far more viable as an alternative to existing control solutions if it could be simply and cost-effectively extended to current-controlled inverters. This is true not only for DZO control, but for any converter control method that assumes voltage-source converters. A general method of extending voltage-source control algorithms to current-controlled converters is therefore developed. This method is subsequently used to apply DZO control to current-controlled inverters.

3.1 Converter Model

The primary difference between voltage-source and current-controlled converters is how the switching patterns of either are controlled: Voltage-source converters track a reference voltage signal and current-controlled converters track a reference current. The ideal version of either type of converter is modeled as a source, where the switching dynamics are neglected and the output is always exactly equal to the control input.

A typical voltage-source converter is shown in Figure 6. The semiconductors are shown as ideal switches. The voltage at the output of the inverter bridge is V_i, and current is measured at that location. The converter has an output filter with an inductor and a parallel capacitor, which is sometimes omitted depending on filtering requirements. The "Grid" component G reflects everything else in the system: impedances, loads, and other inverters. It establishes a voltage V_G based on the injected current and activity in the rest of the system. While a single-phase inverter is shown here, other switch configurations can create three-phase inverters as well [12].

This system can be simplified by assuming the switching dynamics are fast enough to be neglected and treating the inverter bridge as an ideal voltage source [12]. The inductor or any series output filter element is reflected in the system F_s which takes voltage drop $V_i - V_G$ as input and calculates a current. The output capacitor or parallel filter elements are lumped into the grid system, now denoted G'. Figure 7 is an example of such a system with closed-loop PI control of the ideal voltage source.

3.2 Voltage-source analysis

Stability analysis of a DC or AC interconnected converter system includes assumptions about three elements: the controller dynamics, the grid impedance and interconnections seen from the voltage source, and the switching dynamics, which are fast and often neglected [12]. The controller

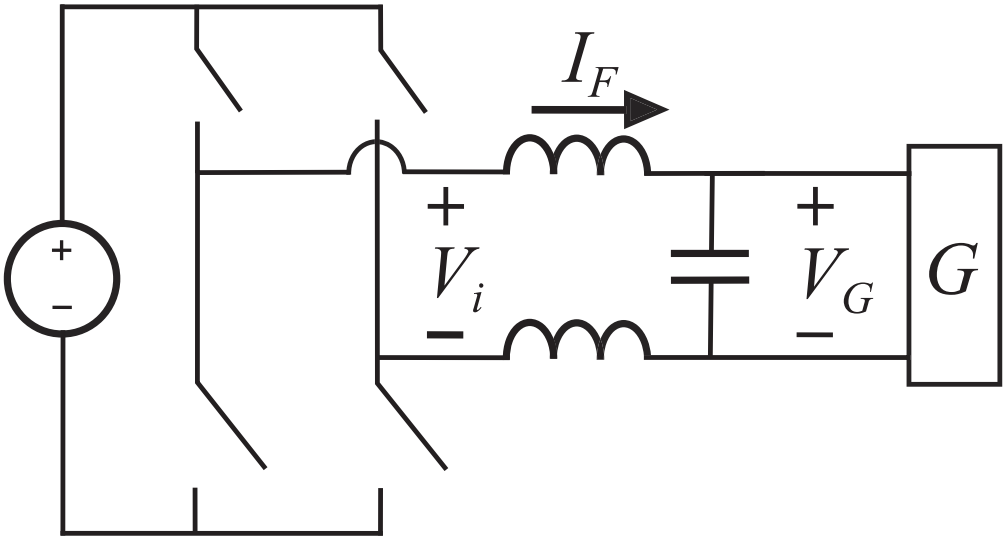

Figure 6: General model of voltage-source converter

dynamics operate in software as $C(I_F)$ and assign a voltage based on the measured output current I_F. The output filter system F_s uses the voltage drop to produce a current. Note that all the components C, F, and G may be nonlinear [12]. The basic equations are thus

$$V_i = C(I_F). \tag{11}$$
$$I_F = F_s(V_i - V_G) \tag{12}$$
$$I_F = F_s(C(I_F) - G'_j(I, u_{1-N})) \tag{13}$$

where the nonlinear F_s in (12) becomes a simple impedance calculation in the linear case.

3.3 Current-controlled equivalent

To change the analysis for a current-controlled version, we assume an arbitrarily fast PI (or similar) current control loop has been designed to enforce a desired output current by varying the bridge output voltage. The grid impedance seen from the terminals of the converter must be bounded [12]. Current-based control requires some ability to modulate output current and will not function with an open circuit. This condition can be satisfied with a parallel-connected filter capacitor as in Figure 6 even if the grid interface to the converter terminals G is unconnected [12]. For an ideal current-controlled converter this would remove the effects of F_s on current as it is within the closed-loop portion. However, we can simulate the effects of any F'_s in software, as shown in Figure 7.

We take the controller output V'_i, and subtract the measured terminal voltage V_G to create the voltage difference needed to calculate output current with F'_s. This current is then fed back as the current command I'_F. Assuming the current controller is very fast and well-tuned, a singular perturbations argument allows us to treat it as a current source so that I_F matches exactly the desired I'_F [12]. We can then replace the closed-loop current controller with a current source for analysis, as in Figure 8.

For a voltage-source model, the output impedance includes the series output filter of the inverter F_s in Figure 7, which is a physical hardware component. For the current controlled version, the

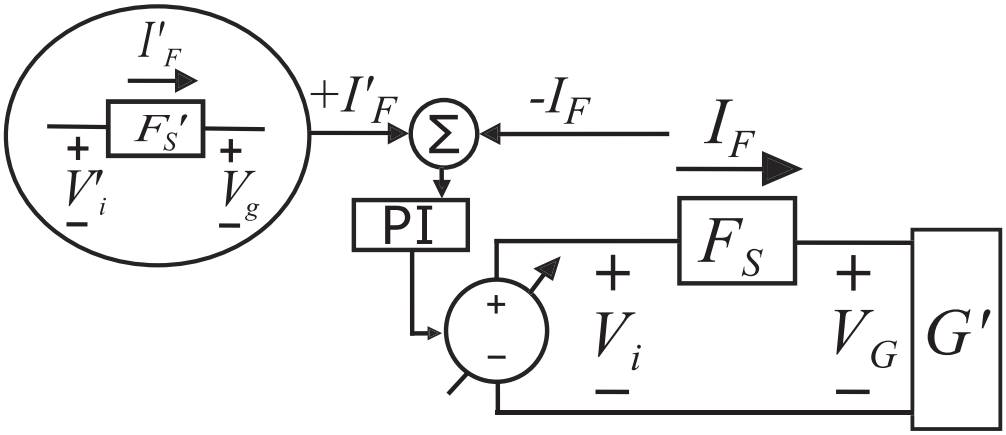

Figure 7: A sufficiently fast closed-loop PI controller on the output of the voltage-source inverter can effectively turn it into a current-source inverter.

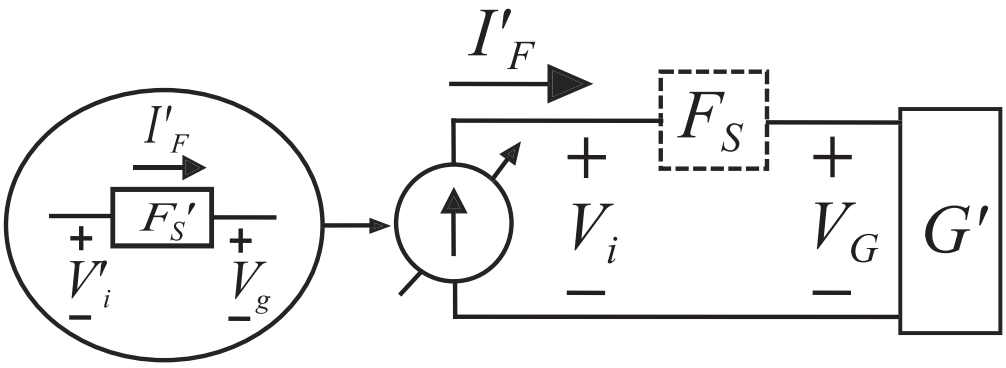

Figure 8: A current-controlled inverter with a sufficiently fast PI loop can enforce any I'_F. Thus, given a simulated output voltage V'_i, it can enforce any $F'_s(V'_i - V_G)$. Note that when $F'_S \neq F_s$, in general $V'_i \neq V_i$.

physical output filter impedance is neglected due to the ideal current control loop, but a simulated filter impedance is included in the controller dynamics. This makes the full system analysis identical to the previous case, except one component is now virtual rather than real. This leaves our modified system:

$$V'_i = C(I'_F) \tag{14}$$
$$I'_F = F'_s(V'_i - V_G) \tag{15}$$
$$I'_F = F'_S(C(I'_F) - G'_j(I, u_{1-N})), \tag{16}$$

with the simulated or virtual quantities denoted by primes [12]. Thus, for $F'_s = F_s$, the system dynamics are identical to the voltage sourced case, except the filter dynamics F'_s are simulated. This method makes no assumptions about linearity or AC vs DC operation. The main underlying assumption is that the current loop is stable and much faster than other dynamics such that I_F converges to I'_F. A necessary condition for this assumption is the effective grid impedance seen from the terminals of the converter must be finite.

As the filter dynamics are now virtual rather than real, this presents two opportunities. Firstly, some methods use the design of this filter to control power sharing, droop, and other converter

behaviors. For this reason, software control of this parameter can be more useful than changing the actual hardware values. Most causal filter models can be used independent of the actual hardware [12]. As a side benefit, the simulated filter impedance will be accurately known for analysis, which is not always the case with hardware systems. This idea similarly extends to three-phase systems, including unbalanced or nonlinear three-phase.

3.4 Adaptation of DZO control to current-controlled inverters

DZO control can be adapted to current-controlled inverters by the method developed in Section 3.1-3.3. As Figure 9 illustrates, the DZO command voltage V_i' is used with the voltage measured at the grid terminal to calculate I_F', which is both sent to the current-controlled inverter as a control signal and fed back into the DZO model to determine the value of V_i' at the next time-step.

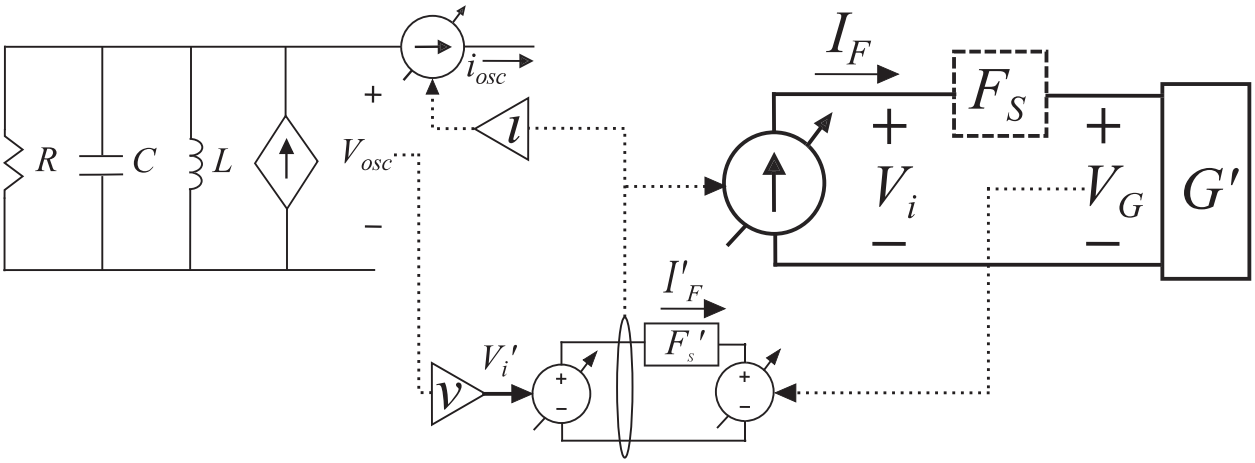

Figure 9: For DZO control of a current-controlled inverter the reference current I_F', rather than measured current I_F, is the feedback signal. I_F' is computed by calculating the current $F_s'(V_i' - V_G)$, Where F_s' represents a simulated output impedance. For an ideal current source, I_F' and I_F are identical.

As implied by Figure 9, the output current of the current-controlled inverter depends on the virtual output impedance F_s', rather than the physical output impedance F_s. As a consequence, the load-sharing results that were achieved by altering F_s in [8] can be replicated by tuning F_s' in the case of current-controlled inverters, rather than by physically changing the inverter output impedances.

4 DZO Control Implementation with Parallel Three-Phase Current-Controlled Inverters

A hardware test bed was designed and constructed as a platform for demonstrating the application of voltage-source algorithms to current-controlled converters as developed in Section 3, and validating DZO control for three-phase systems. This is the first hardware implementation of DZO control either in a three phase system or with current-controlled inverters, so its performance under a single set of control parameters is evaluated.

4.1 Test bed overview

The three-phase testbed consists of three current-controlled inverter units connected in parallel to a wye-connected resistive load. Figure 10 shows one inverter unit connected to the load, and displays the core functional elements of the unit. Figure 11 shows the full test bed. Figure 12 displays a mechanism for applying step-changes to the system load.

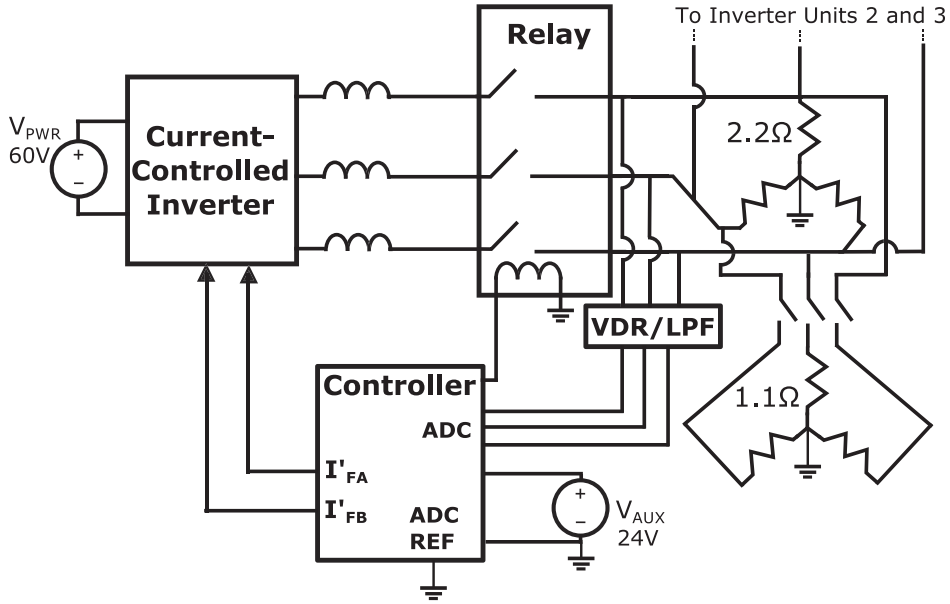

Figure 10: One three-phase, current-controlled inverter unit coupled to a wye-connected load. The inverter's control signal reference and its negative DC rail are isolated. The negative DC power rail of each inverter floats in isolation. Each inverter unit's controller reads $V_{G,A}$ and $V_{G,B}$, the load voltages on phases A and B. Additional inverter units are connected in parallel to the load for synchronization testing.

Each inverter is powered by a floating 60V DC power source. The inverter units are sized to the current ratings of the inverters, which enforce a protective limit of 25A on per-phase output current. The control parameters of each inverter are tuned so that the steady-state per-phase output current amplitude of one inverter coupled alone to a three-phase, 2.2 Ω load is approximately 2A peak-to-peak, corresponding to a power output of approximately 13.2 W. The signal and power circuits of each inverter are isolated from one another. The inverter's control signal circuit and the controller itself are both grounded to the system neutral line, which is earth-grounded. A 24V DC power source powers each unit's controller and inverter-cooling fan, and serves as the driving source for the power relay that connects and disconnects the inverter unit from the system.

4.2 Interface board design

An interface board streamlines and reinforces system interconnections between the controller, inverter, and power lines of each inverter unit. Its functions include 1) controller protection, 2) noise filtering, and 3) remote inverter connection/disconnection. The interface board is shown in Figure 14b, and its basic functions are outlined in brief below:

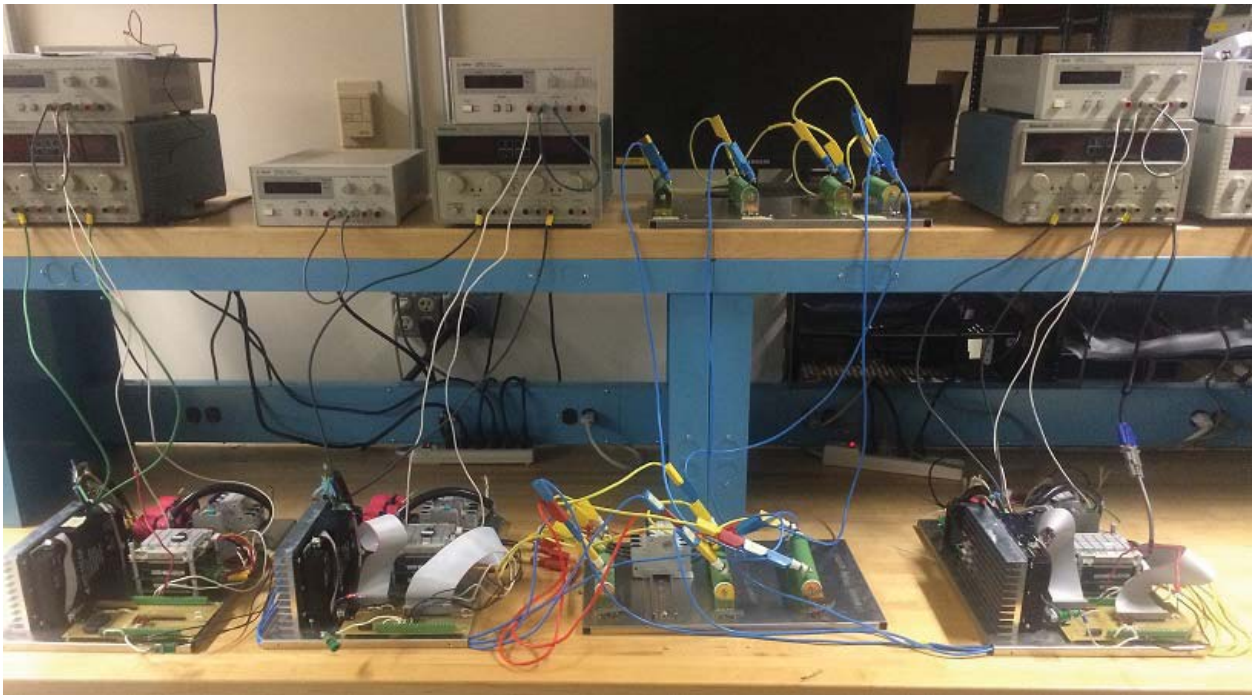

Figure 11: The testbed comprises three inverter units connected in parallel to a wye-connected three-phase load, shown in the center of the picture on the lower shelf adjacent to the inverter modules. DC power sources are on the upper shelf, providing power to the inverter subunits.

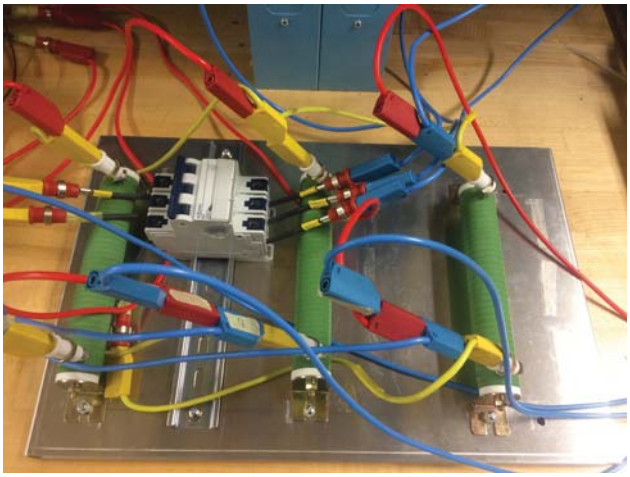

Figure 12: The testbed's wye-connected load includes a hand-thrown switch that allows the resistance of the load to be quickly changed. The open-switch phase resistance of the load is 2.2 Ω and the closed-switch resistance is 0.733 Ω.

4.2.1 Voltage measurement

The controller samples $V_{G,A}$ and $V_{G,B}$, each at a rate of 10kHz. A low-pass filter was necessary to ensure the stability of the controller dynamics in the presence of switching noise. A combined low-pass filter and voltage divider, illustrated topologically in Figure 13, was designed to scale system voltages to within the range of the controller's analog-to-digital ports and to attenuate switching noise.

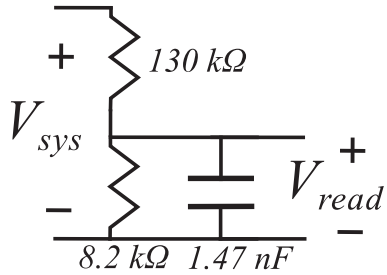

Figure 13: A combined voltage-divider and low-pass filter scales system voltages down to levels within the controller's range and filter channel noise and switching harmonics

The purpose of the voltage divider is to ensure that the entire range of possible system voltages are scaled down to within the measurement range of the controller. In this test bed, the measurement range of the controller is $\pm 10V$. Thus, the purpose of the voltage divider is to scale $V_{sys,max}$, the maximum possible system voltage, such that (17) is satisfied. If an overhead margin of 25% is imposed on the $\pm 10V$ measurement range, then we have

$$|V_{read,max}| = \left| V_{sys,max} \frac{R_L}{R_L + R_U} \right| \leq 7.5V \tag{17}$$

Where V_{sys} is the system voltage being measured and V_{read} is the value of the system voltage after being scaled by the voltage divider comprising R_L and R_U. $V_{sys,max}$ is calculated for the case in which the controller and the negative DC rail of the inverter are grounded together, and the three-phase neutral line is isolated. The controller measures the voltage difference between the phases of the system load and ground, so to size the voltage divider appropriately V_{sys} is set equal to the maximum phase-to-ground voltage.

The phase-to-ground voltage is equal to $V_{pn} + V_{ng}$, the sum of the phase-to-neutral and neutral-to-ground voltages. It follows, if V_{pn} and V_{ng} are assumed to vary independently, that

$$V_{sys,max} = \max(V_{pn}) + \max(V_{ng}) \tag{18}$$

The inverter DC rail voltage V_{DC} is the maximum line-to-line voltage that can be imposed on the load, so $\max(V_{pn}) = V_{DC}/\sqrt{3}$ if balanced three-phase voltages are assumed. The maximum value of V_{ng} is equal to V_{DC} due to the common-mode voltage of a switched three-phase inverter. Thus,

$$V_{sys,max} = V_{DC,max} \left(1 + \frac{1}{\sqrt{3}} \right) \tag{19}$$

Some bound must be placed on V_{DC} because if the voltage divider is designed to scale arbitrarily large voltages down to within an acceptable range for the controller then system voltages of interest will be scaled down too much to be effectively resolved. As such, the voltage divider is sized for $60V \leq V_{DC} \leq 80V$.

If we set $V_{DC} = 80V$ and substitute $V_{sys,max}$ into (17), then we have

$$\frac{R_L}{R_L + R_U} \approx 0.059 \tag{20}$$

Although any values of R_L and R_U that satisfy (20) would scale the system voltage appropriately, selecting very high resistances relative to the system load results in less of a loading effect on the system by the voltage divider. To that end, R_L and R_U are chosen to have resistances of $8.2k\Omega$ and $132k\Omega$, respectively.

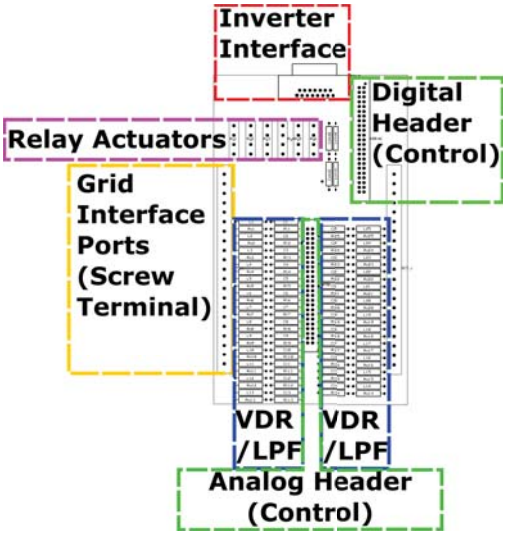

(a) Interface board Schematic

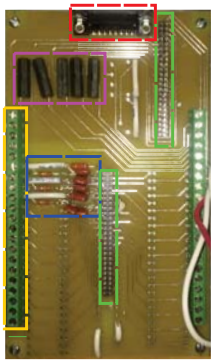

(b) Completed Interface board

Figure 14: Realization of an interface board for the DZO hardware test bed. a) Interface board schematic highlights the main functional blocks of the inverter. The un-indicated components to the right of the Relay Actuators are low-pass filters for the control signals and are not in use, b) A completed interface board with three voltage-divider/low-pass filter channels for reading the voltage on each phase of the inverter it controls. This interface board is fitted with several silicon-controlled relays so that it can actuate not only its own power relays but also those of other inverter units.

As is displayed in Figure 15a, the primary noise frequencies of the test bed are $56.5kHz$ and $113kHz$. This channel noise was found to cause instability in the operation of a three-phase current-controlled inverter under DZO control. The purpose of the low-pass filter is to attenuate this channel noise in order to enable the stable operation of inverters under DZO control. The voltage divider circuit is modified to include first-order low-pass characteristics by adding a capacitor in parallel with R_L, as is displayed in Figure 13. The gain and phase-delay characteristics of the low-pass filter are shown in Figures 15b and 15c for a filter capacitance value of $1.47nF$.

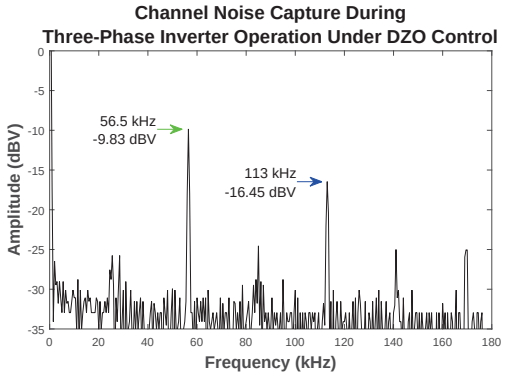

(a) The two primary noise frequencies in the testbed occur at 56.5 kHz and 113 kHz. The operation of switched inverters creates noise at frequencies that are harmonically related to the switching frequency.

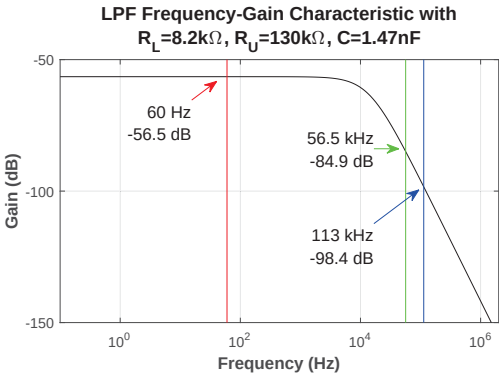

(b) Signals at the frequency of DZO oscillation (60Hz) are in the passband of the LPF and the lowest-frequency, most significant noise signal at 56.5 kHz is attenuated by approximately 28.4 dB

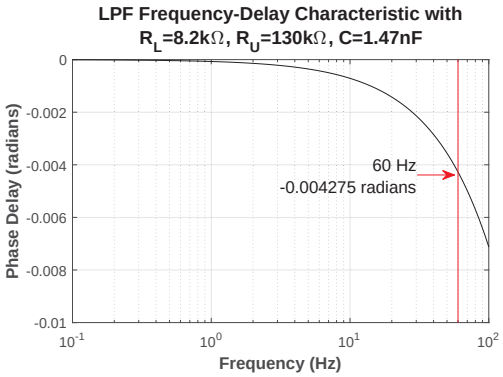

(c) The phase delay imparted to a 60Hz signal by the LPF as designed is 0.004275 radians, corresponding to a time-delay of approximately 11.3 μs for a 60Hz sinusoid. System stability with this amount of delay in the voltage measurement was confirmed in simulation before implementing the LPF in hardware.

Figure 15: A first-order low-pass filter

4.2.2 Inverter on/off switching

Each inverter unit's controller actuates a normally-open relay to connect the unit to the grid. When the relay is open the controller holds the states of the simulated DZO, as well as $I'_{F,A}$ and $I'_{F,B}$ at zero to prevent current loop saturation. Each interface board includes several silicon-controlled relays to allow the controller to actuate large relays whose coil requirements exceed its driving capacity.

4.2.3 Controller multi-compatibility

The interface board is designed to be compatible with two different controllers, so that the design of additional inverter units for the test bed can be scaled sensibly to match performance requirements. The board can be prepared for use with either controller by scraping 3-5 traces off the board.

5 Experimental Results

This section demonstrates two concepts. The first is the synchronization of parallel-connected inverters, and the second is the ability to dynamically control load-sharing between inverters. As developed in Section 3.4, the power output of any current-controlled inverter under DZO control can be modified by changing the virtual output impedance used to compute its output current. This demonstration also serves as a first hardware validation for DZO control of power systems comprising three-phase, current-controlled inverters.

5.1 Inverter Synchronization

The ability of an inverter under DZO control to synchronize with a network of inverters upon connection is demonstrated. Current measurements for each phase of each inverter are displayed in Figures 16a and 16b. Notable features of this process include: a) Current spike approximately 10ms after the synchronizing inverter is connected, reaching a maximum of 4.64A on one phase. b) Out-of-phase oscillation from 10ms-200ms after connection. c) Low-amplitude oscillation of the synchronizing inverter from 200ms-250ms. d) Convergence to full-amplitude, in-phase oscillation after 250ms.

5.2 Inverter load-sharing control through manipulation of virtual output impedance

The virtual output impedance of an inverter can be manipulated during operation to change that inverter's share of the load. In the test demonstrated by Figure 17a, both inverters oscillate in steady-state synchronization with identical virtual output impedances ($Z'_{F,1} = Z'_{F,2}$) until κ_2 is doubled at time 0, increasing $|Z'_{F,2}|$ to twice $|Z'_{F,1}|$. After κ_2 is doubled, the output currents $I_{F,1}$ (Red) and $I_{F,2}$ (Green) continue to oscillate in phase but $|I_{F,2}|$ is approximately half of $|I_{F,1}|$. This observation is consistent with the expectation developed in (9). The opposite process, in which κ_2 is halved rather than doubled, is shown to also yield the expected results in Figure 17b, with $|I_{F,2}|$ increasing to approximately twice $|I_{F,1}|$.

5.3 Response of inverters to a step-change in load

The stability through rapid step-changes in load of parallel-connected, current-controlled inverters under DZO control was assessed by switching the load resistance from 2.2 Ω to 0.733 Ω (66% decrease) on each phase while two inverters were oscillating in steady-state synchronization. In Figure 18a, two synchronized inverters with equal load share ($Z'_{F,1} = Z'_{F,2}$) are subjected to the load change. Figure 18b shows the same step change in load resistance applied to inverters with unequal sharing ($Z'_{F,1} = 2Z'_{F,2}$) such that the load-share of the first inverter (Red) is half that of the second inverter (Green). It can be seen for both tests in that the inverter output currents maintain both their relative amplitudes and their phase synchronization during a step change in load resistance from 2.2 Ω to 0.733 Ω.

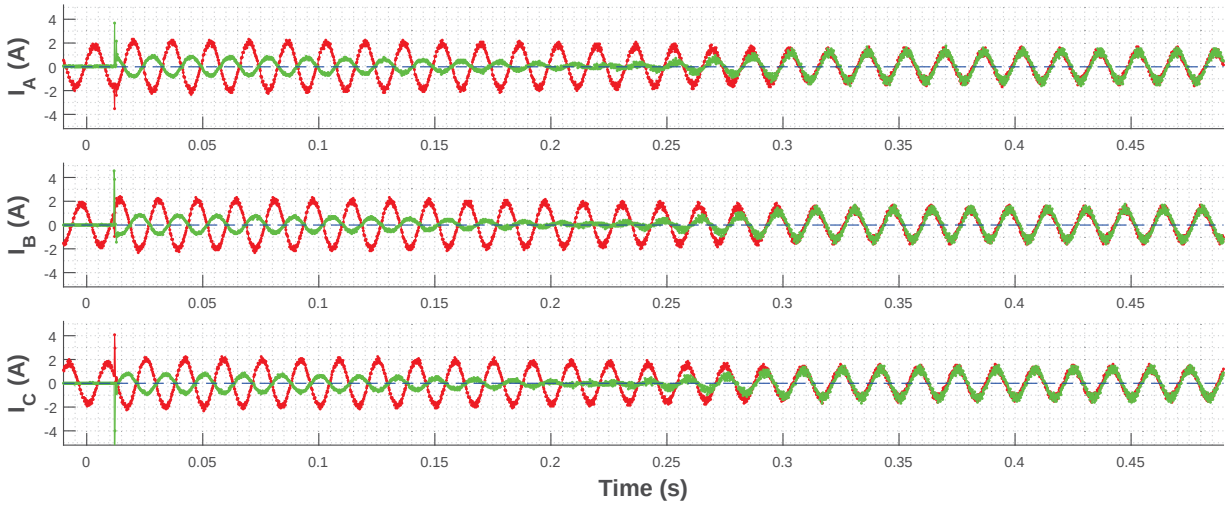

(a) Current-source inverter synchronizes when connected to another inverter.

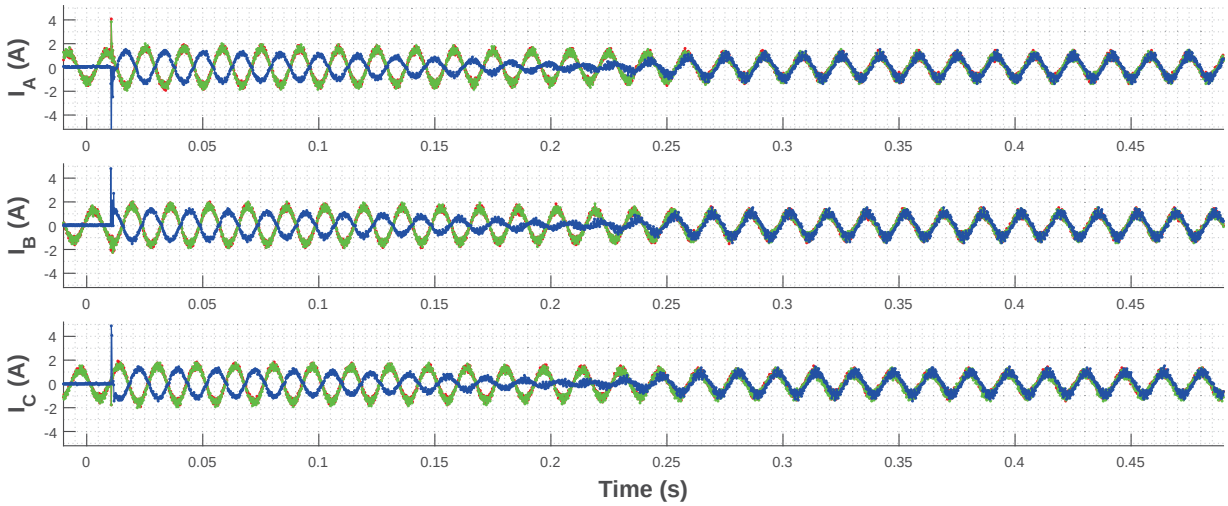

(b) Current-source inverter synchronizes when connected to two already-synchronized inverters.

Figure 16: Two test cases demonstrate the effectiveness of DZO control in synchronizing three-phase current-controlled inverters.

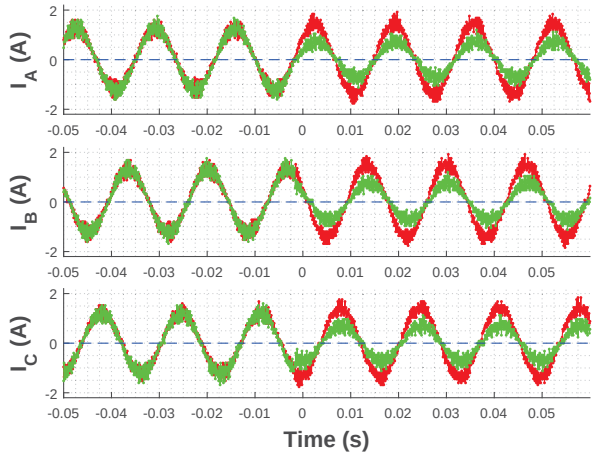

(a) The load carried by one inverter is decreased by increasing virtual output impedance

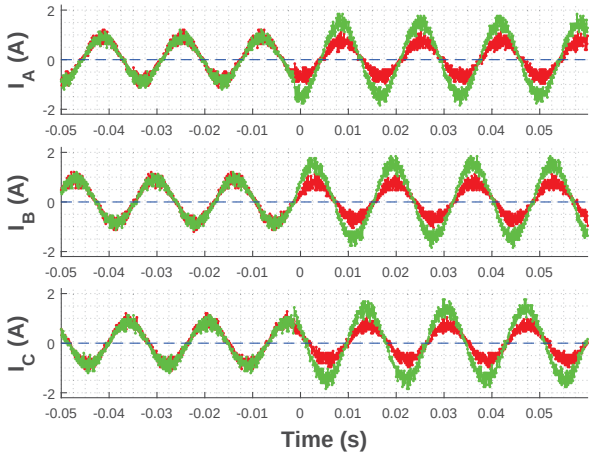

(b) The load carried by one inverter is decreased by increasing virtual output impedance

Figure 17: Three phase test cases demonstrate the ability to control load sharing between two different inverters by changing the virtual output impedance of one of them.

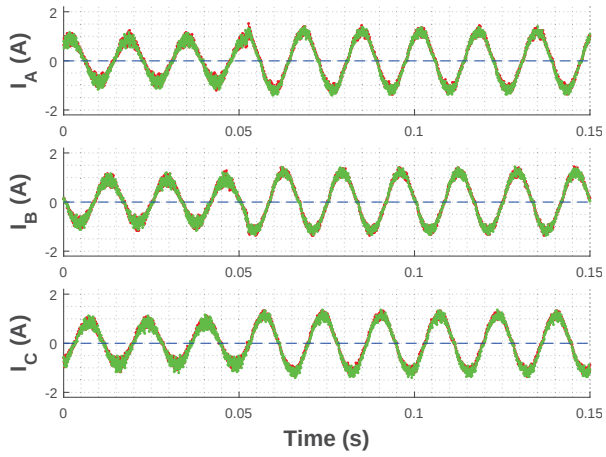

(a) Inverters with equal power sharing

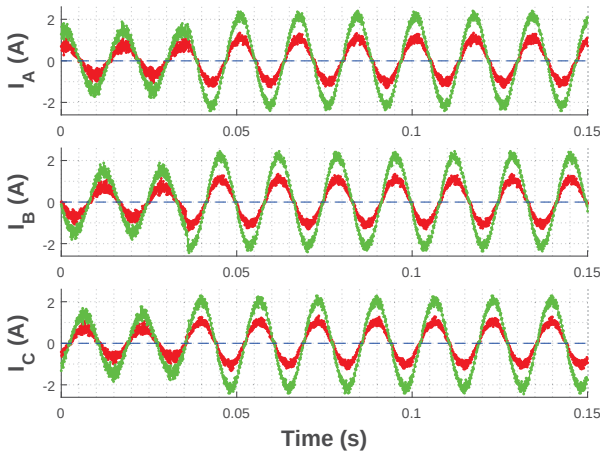

(b) Inverters with unequal power sharing

Figure 18: Two synchronized inverters, with both equal and unequal load-sharing, maintain their behavior through a step increase in load. Load resistance changes from 2.2 Ω to 0.733 Ω

6 Conclusions

An approach to power electronic converter control that bridges the gap between voltage-source and current-controlled converter applications was formulated and validated experimentally by the implementation of Dead-Zone Oscillator control with current-controlled inverters. DZO control was experimentally validated for the first time in a three-phase grid and with current-controlled inverters. The unique ability of current-controlled inverters to tune their effective output impedances was demonstrated, and one potential advantage associated with this ability was demonstrated by dynamically changing the load-share of parallel-connected current-controlled inverters during operation. The robustness of DZO control to a 66% step-change in load was also demonstrated, both with equal and unequal load-sharing configurations. These results will facilitate the deployment of DZO control, both by extending it to three-phase, current-controlled inverter networks and by demonstrating a previously unexplored method of controlling inverter load-sharing.

References

[1] A. Bidram, F. Lewis, and A. Davoudi, "Distributed control systems for small-scale power networks: Using multiagent cooperative control theory," *IEEE Control Syst. Mag.*, vol. 34, no. 6, pp. 56–77, 2014. [Online]. Available: http://ieeexplore.ieee.org/stamp/stamp.jsp?arnumber=6915832

[2] D. Trudnowski, M. Donnelly, and E. Lightner, "Power-system frequency and stability control using decentralized intelligent loads," in *Transmission and Distribution Conference and Exhibition, 2005/2006 IEEE PES*, 2006, pp. 1453–1459. [Online]. Available: http://ieeexplore.ieee.org/stamp/stamp.jsp?arnumber=1668732

[3] B. Dong, Y. Li, Z. Zheng, and L. Xu, "Control strategies of microgrid with hybrid DC and AC buses," in *Power Electronics and Applications (EPE 2011), Proceedings of the 2011-14th European Conference on*, 2011, pp. 1–8. [Online]. Available: http://ieeexplore.ieee.org/stamp/stamp.jsp?arnumber=6020119

[4] V. Salehi, A. Mohamed, and O. Mohammed, "Implementation of real-time optimal power flow management system on hybrid AC/DC smart microgrid," in *Industry Applications Society Annual Meeting (IAS), 2012 IEEE*, 2012, pp. 1–8. [Online]. Available: http://ieeexplore.ieee.org/stamp/stamp.jsp?arnumber=6374113

[5] B. Johnson, S. Dhople, A. Hamadeh, and P. Krein, "Synchronization of nonlinear oscillators in an LTI electrical power network," *IEEE Trans. Circuits Syst. I*, vol. 61, no. 3, pp. 834–844, 2014. [Online]. Available: http://ieeexplore.ieee.org/stamp/stamp.jsp?arnumber=6701226

[6] F. Dörfler, M. Chertkov, and F. Bullo, "Synchronization in complex oscillator networks and smart grids," *Proceedings of the National Academy of Sciences*, vol. 110, no. 6, pp. 2005–2010, 2013.

[7] J. W. Simpson-Porco, F. Dörfler, and F. Bullo, "Synchronization and power sharing for droop-controlled inverters in islanded microgrids," *Automatica*, vol. 49, no. 9, pp. 2603–2611, 2013.

[8] B. Johnson, S. Dhople, A. Hamadeh, and P. Krein, "Synchronization of parallel single-phase inverters with virtual oscillator control," *IEEE Trans. Power Electron.*, vol. 29, no. 11, pp. 6124–6138, 2014. [Online]. Available: http://ieeexplore.ieee.org/stamp/stamp.jsp?arnumber=6692879

[9] B. Johnson, S. Dhople, J. Cale, A. Hamadeh, and P. Krein, "Oscillator-based inverter control for islanded three-phase microgrids," *IEEE Journal of Photovoltaics*, vol. 4, no. 1, pp. 387–395, 2014. [Online]. Available: http://ieeexplore.ieee.org/stamp/stamp.jsp?arnumber=6620994

[10] F. Dörfler and F. Bullo, "Synchronization in complex networks of phase oscillators: A survey," *Automatica*, 2014.

[11] A. Yazdani and R. Iravani, *Voltage-Sourced Converters in Power Systems*, 2010.

[12] D. F. Opila and S. C. Shabshab, "Extending control stability results from voltage-sourced to current-controlled ac or dc power converters," in *International Federation of Automatic Control, 2016*.